RSC Advances

RSC Publishing

PAPER

Identifying emerging trends of protein hydrogels for biological scaffolding†

Cite this: *RSC Adv.*, 2013, **3**, 24256

Paula V. Messina,[a] Natalia Hassan,[be] Armando Soltero[c] and Juan M. Ruso*[d]

The strategies of bottom-up design of inorganic structures from biological templates enable cheap, eco-friendly and efficient fabrication of nano-structured materials. Here, template assembly of silica nanostructures were achieved using different protein hydrogels. Ovalbumin and fibrinogen gels were prepared by heat treatment at different pHs and protein concentrations. These hydrogels have been morphologically (SEM) and mechanically (rheology) well characterized. Next, a silica precursor is added, the condensation reaction is initiated and finally the protein hydrogel template is removed by calcination. A variety of 3D nanostructures ranging from highly porosity structures to spherical particles have been identified and characterized. Furthermore, it was observed that the fractal dimension of silica structures follow the same pattern than their corresponding templates. Consequently, the bio-scaffolding method proposed here helps the bottom-up assembly of silica precursors in nanostructures with defined three dimensional dimensions and provides a versatile route for the design of new architectures under green conditions.

Received 3rd May 2013
Accepted 10th October 2013

DOI: 10.1039/c3ra42204f

www.rsc.org/advances

1. Introduction

If the incorporation of new technologies and more efficient methods is a common practice in all fields of science, it has been precisely in the study of biotechnology where the innovation has achieved impressive proportions. One of the current trends in biotechnology concerns the creation of structures combining organic and inorganic materials in a synergistic way.[1] Thus, bioinspiration is all around us. Biomineralization is the process by which biological organisms are directly involved in the synthesis of inorganic materials:[2,3] peptides,[4] urchins[5] or vertebrates.[6,7] Bioconjugation refers to the covalent derivatization of biomacromolecules. Biotemplating, involves the formation of inorganic materials using natural materials as scaffolds.[8] Such interest is motivated primarily by the desire to simultaneously exploit the properties of both inorganic and biological components in new hybrid devices or materials that can be applied in areas ranging from energy harvesting and nanoscale electronics to biomedical diagnostics.[9,10] The utility and effectiveness of these composites will be predicated on the ability to assemble these structures with control over organic/inorganic ratio, biomolecular orientation, biomolecular activity, and the separation distance within the compounds architecture.[11] As a result, biological scaffolding reduces the complexity of the templates and can create a great variety of materials for a cheaper cost.

The ability to form gels is an important protein function. Most protein gels are formed by denaturation, aggregation, and gelation during the heating process. In these systems, the network is cross-linked by transient, noncovalent associations such as hydrophobic interactions, chain entanglements, hydrogen bonds or ionic bonds. Bulk mechanical properties are governed at the molecular level by the strength and number of these transient interactions. In terms of biotemplating, the hydrogel template strategy addresses various issues associated with the fabrication of nanostructures. The formed nanostructures can be easily collected by simply calcinations or dissolving the template. Further, certain hydrogels, such as gelatin, form phase-reversible elastic and mechanically strong hydrogels that can withstand physical manipulation during template preparation and filling.[12,13] Finally, the hydrogel template strategy is cheap, eco-friendly, and it can be easily scaled up for industrial application. However, the key issues with these techniques are the control of particle size and prevention of agglomeration and nano-reproducibility, which are very important in application.

[a]*Department of Chemistry, Universidad Nacional del Sur, INQUISUR-CONICET, 8000 Bahía Blanca, Argentina*

[b]*Laboratoire Physico-chimie des Electrolytes, Colloides et Sciences Analytiques (PECSA), Université Pierre et Marie Curie, 75252 Paris, France*

[c]*Departamento de Ingeniería Química, Universidad de Guadalajara, Guadalajara, Jalisco, 44430 Mexico*

[d]*Soft Matter and Molecular Biophysics Group, Department of Applied Physics, University of Santiago de Compostela, Santiago de Compostela, 15782, Spain. E-mail: juanm.ruso@usc.es; Tel: +34 981563100*

[e]*Laboratorio de Nanobiotecnología, Facultad de Ciencias Químicas y Farmaceuticas, Universidad de Chile, Chile*

† Electronic supplementary information (ESI) available: Fig. S1. See DOI: 10.1039/c3ra42204f

Despite some initial work,[14–16,17] the possibility of using these proteins hydrogels directly to design nanomaterials remains virtually untapped. Consequently, interest in developing diverse inorganic nanostructures from biological templates continues to grow almost unabated. Hence, our aim in this article is to build upon the knowledge in this area in several ways. On one hand, we are trying to clarify how the mechanical properties and geometry of the gels affect the formation of siliceous nanostructures and, on the other hand, we are trying to enhance the catalytic role of the protein structure. For this purpose, we have chosen ovalbumin and fibrinogen.

Ovalbumin,[17] a major component of egg white proteins, has important implications in food systems improving sensory perception.[18,19] This protein is grouped into the serine proteinase family inhibitors, which controls serine proteinases involved in diverse physiological reactions, because of the close similarity in the primary and tertiary structures. It has a molecular weight of 45 000 Da and consists of a single chain of 385 amino acids with 105 titrable residues,[20] containing a single disulfide bond (interconnecting two parts of the chain) and a glycosylation (mainly mannose) site. Three different ovalbumin phosphate forms containing two, one or zero phosphate groups per molecule (85 : 12 : 3 ratio respectively) occur in egg white. This protein presents a globular shape with a radius of $\approx$3 nm in an aqueous medium and an isoelectric point (pI) at pH 4.6.[21] When stored for extended periods of time, or by heat processing, the native *R*-ovalbumin converts to *S*-form that is more resistant to denaturation by heat, urea, or guanidine.[22] The ovalbumin globules are also known to make a self-organized mesoscopic structure, which is governed by several factors: temperature, concentration or electrolyte.[23] To effectively control and optimize this process, a deep understanding of how external factors influence protein morphology is essential. Interests of the industry in ovalbumin hydrogels range from emulsifying activity (it is higher at acidic pH) to drug delivery systems. Also, acid-sensitive microgels for the development of protein-based vaccines under acidic conditions, like those found in the phagosomes of antigen-presenting cells, are highly demanded.[24]

Fibrinogen is a complex multidomain protein whose major function is to form fibrin clots that prevent the loss of blood upon vascular injury. Bovine fibrinogen (340 kDa) is a 45 nm long (with an approximate diameter of 5 nm) disulfide-linked dimer of three nonidentical polypeptide chains, Aα, Bβ, and γ. The NH_2 terminal portions of the six chains are linked together in the central region of the molecule by 11 disulfide bonds forming a small globular domain, the so-called disulfide knot, in the center.[25,26] The C termini of each of the three chains end in globular domains, those of the Bβ and γ chains are located at the ends of the molecule. Cleavages in all three chains then yield two D domains and one E domain. The E domain consists of the NH_2-terminal regions of α-, β-, and γ-chains chains held together by disulfide bonds. The majority of the D region is formed by the C-terminal portions of the β- and γ-chains folded into similar structures. The COOH-terminal portion of each fibrinogen Aα chain forms a compact αC-domain attached to the bulk of the molecule with a flexible αC-connector. In addition, fibrinogen shows a unique characteristic in its folding. According to the current view, two αC-domains in fibrinogen interact intramolecularly with each other and with the central region of the molecule. In contrast, in fibrin they switch to an intermolecular interaction to form αC-polymers. This structural organization drives the fibrin assembly process and promotes cell adhesion and migration through RGD sequences.[27] Recent studies have focused on the complexation of fibrinogen with ligands, including surfactants and drugs, and on their adsorption behavior at different interfaces.[28–31] These studies use a combination of experimental techniques to enable the complete characterization and understanding of the physicochemical phenomena involved in these interactions. The physicochemical properties of the hydrogel formed from physically cross-linked fibrinogen molecules have been recently reported.[32] However, most studies have been performed in the presence of thrombin. Through proteolytic cleavage, this enzyme converts fibrinogen into insoluble strands of fibrin and drive gelation.

The physicochemical properties of these hydrogel were evaluated by using rheological measurements that are easy to conduct, especially in the high concentration range of proteins.[33] The structure and geometries of the gels and materials formed were obtained by scanning and transmission electron microscopy.

2. Materials and methods

2.1. Materials

Ovalbumin (Albumin, Chicken Egg, product A-5253, Sigma Chemical Company) was used without further purification. Bovine plasma fibrinogen, fraction I, type IV (product F8630), was purchased from Sigma and used without further purification. Thrombin for bovine plasma lyophilized powder (Factor IIa, product T4648) was purchased from Sigma Aldrich. Sodium tetraethyl orthosilicate (TEOS, Aldrich, 98%) were used without further purification. Sodium metasilicate (Aldrich, 95%). All chemical reagents were of analytical grade, and solutions were made using doubly distilled and degassed water.

2.2. Synthesis of ovalbumin and fibrin hydrogels

For the preparation of ovalbumin hydrogels the protein solutions at different concentrations (20, 40 and 80 g L^{-1}) were dissolved in water, pH was adjusted to pH 3 with HCl 0.1 M, and in the case of pH 10 was adjusted with NaOH 0.1 M. The solutions were stirred for 2 hours until the hydrogel formation. Fibrin hydrogels were prepared dissolving fibrinogen (concentration) in phosphate buffered saline (pH 7.4) and stirring for 30 min, after this time was added 10 NIH per mL of thrombin (2 g L^{-1}, 4 g L^{-1}, 6 g L^{-1}, 8 g L^{-1}) and the mixture was stirred for another 30 min.

2.3. Synthesis mesoporous silica materials

Depending on the pH of the hydrogel preparation, different syntheses were essayed. First and according to a previous descript procedure for the synthesis of siliceous materials on

basic conditions,[34] for ovalbumin hydrogels at pH 10, 3.05 mL of TEOS was dissolved in 0.52 mL of water and stirred for 10 min at 500 rpm. Then, a solution of 0.25 g of NaOH in 4.5 mL of water was added drop-by-drop to the TEOS solution while stirring. A minute later, the ovalbumin hydrogel were added to the TEOS solution and was stirred for 5 minutes. In the case of hydrogels formed at pH 3 the synthesis was different.[34] A solution of 1.5 g of sodium metasilicate was added to ovalbumin hydrogel at room temperature and was stirred for 10 minutes. To this reaction mixture, 2.57 mL of HCl 37% was quickly added with vigorous magnetic stirring. The resulting mixture was stirred for 1 hour at room temperature. For fibrin hydrogels at pH 7.4, the material preparation was performed by following the same procedure than for ovalbumin hydrogel at pH 10. The resulting products (acids and basics mixtures) were left for 8 hours in an autoclave at 100 °C. The obtained materials were filtered, washed with triple-destilled water, and left to dry at room temperature. Finally, they were calcinated for 7 hours at 600 °C in an air flux.

2.4. Rheology

Rheological experiments were performed on a Bohlin CS-10 stress-controlled rheometer. A Couette geometry (cup 27.5 mm diameter, height 35 mm, gap 5 mm.) with a bob of the Mooney type was used. The cell was heated by a reservoir of fluid circulating from a Julabo thermostated bath. The sample was equilibrated for at least 20 min prior to each experiment. Both steady and dynamic rheological experiments were performed at each temperature. Dynamic frequency sweep measurements were performed in the linear viscoelastic regime of the samples, as determined by dynamic stress-sweep measurements. For the steady-shear experiments, an equilibration time of 90 s was given at each shear stress.

2.5. Field emission scanning electron microscopy (FE-SEM)

Field emission scanning electron microscopy (FE-SEM) was performed using a ZEISS FE-SEM ULTRA PLUS. This instrument operates in high vacuum enabling the collection of high resolution images (0.8 nm at 30 kV) and low voltage (0.02 V–30 kV, continuously adjusted in steps of 10 volts) in samples without shading. The magnification of the images ranged from 12–1 000 000× and the sizes of the openings that were used were 7.5 μm, 10 μm, 20 μm, 30 μm, 60 μm and 120 μm. Local charging was compensated by injection of nitrogen gas.

2.6. X-ray powder diffraction

Powder X-ray diffraction (XRD) data were collected with a Philips PW 1710 diffractometer with Cu-Kα_α radiation (λ = 1.5418 Å) and a graphite monochromator operated at 45 kV; 30 mA and 25 °C.

3. Results and discussion

3.1. Hydrogels characterization

SEM images were obtained to characterize the microstructure morphologies of the hydrogels. The surfaces images of the hydrogels are presented in Fig. 1a–i. Images were chosen as representative of the bulk sample as possible. Improper preparation methods may create artifacts that may be misinterpreted, so the risk of artifacts as results of dehydration of samples for SEM analysis was minimized which ensure quality and integrity of the images. However, the general structure of the gels is still evident and similar to those synthesized with widely used polymers such as polyethylene glycol and polylysine[35] or polyvinyl alcohol with chitosan.[36] Regardless of the protein concentration, these systems produced similar patterns for hydrogels created at the same pH (shown in rows). Two distinct groups were found by comparing the surface structure of the gels. The first group corresponds to those based on ovalbumin at pH 3 whose morphology presents a coarse rough appearance composed of tightly agglomerated particles (images 1a to 1c). The other group is represented by hydrogels produced by ovalbumin at pH 10 (images 1d to 1f) and fibrinogen at pH 7.4 (images 1g to 1i). The morphology of these materials is characterized by a continuous and relatively open 3D network structure where the pores are mostly circular and elliptical in shape with variable interior pore interconnections. The dramatic change in morphology from monolithic agglomerated particles to high 3D porosity shows not only that the hydrogel method can be extended to different applications, but also that systems with the same proteins are themselves very sensitive to changes in experimental conditions. The reason for the change in morphology is not completely clear. However, taking into account that protein-solvent interactions are in competition with protein–protein interactions, being at the pI most favor protein–protein interactions, which leads to precipitation, compared to protein-solvent interactions which lead to solvation. In addition, the partially denaturated proteins due to the pH, can aggregate and, under appropriate conditions, produce a macroscopically continuous three-dimensional gel network that entraps and restricts the motion of the solvent. For this reason, changes in morphology are most probably caused by differences in pH with respect of isoelectric point of the proteins (4.6 for ovalbumin and 5.1 for fibrinogen): the closest to the pI (ovalbumin at pH 3) results in monolithic and compact structures. However, those far from the pI results in more open structures.

Histograms of the average pore area were generated from different SEM images for hydrogels formed at pH 10 (ovalbumin) and pH 7.5 (fibrinogen). The corresponding distribution histograms are shown in Fig. S1 (ESI†). All distributions are unimodal and asymmetrical, with a skewed shape toward the larger areas, characteristic of a lognormal distribution. The histograms illustrate sligh differences in the distribution between all hydrogels. However, there is a significant decrease in the average pore area (obtained from the mode of the pore area distribution) with increasing thrombin protein concentration: from to 15.8 to 8.5 μm^2 in the case of ovalbumin at pH 10 and from 63.6 to 17.1 μm^2 in the case of fibrinogen. Other significant difference among the hydrogels is the wall thickness. It can be observed that an increase in protein concentration causes a decrease in the hydrogel wall thickness. This can be quantified by means of the total area fraction of pores: for example, an increase of total pore area by 7% was observed for

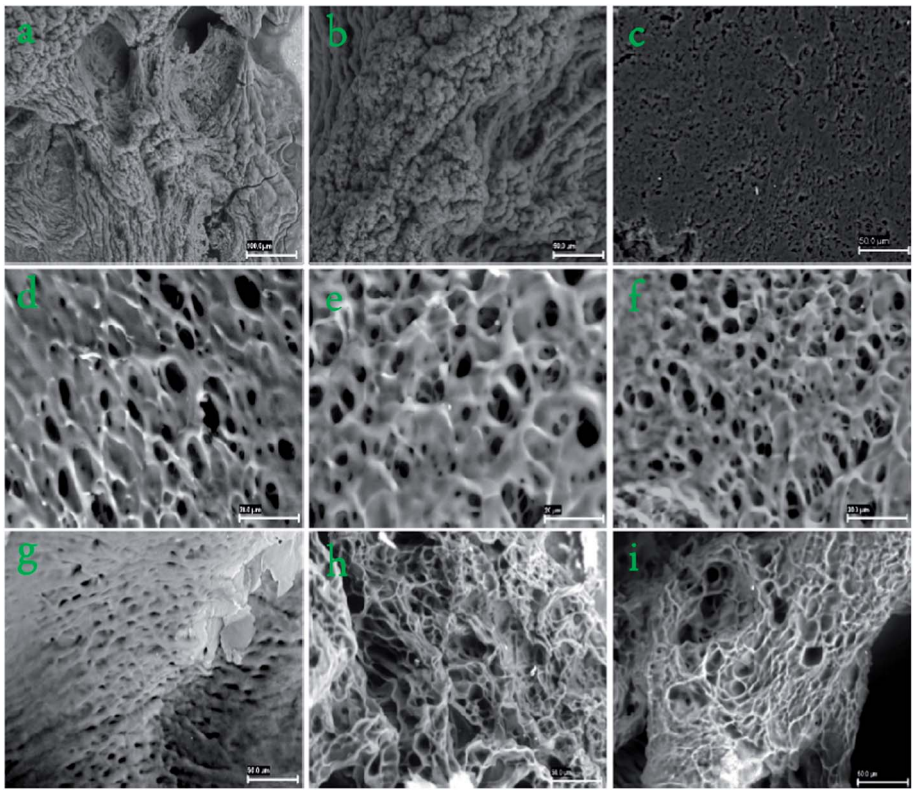

Fig. 1 SEM micrographs of the hydrogels produced at different conditions: (a) ovalbumin 20 g L^{-1} pH 3; (b) ovalbumin 40 g L^{-1} pH 3; (c) ovalbumin 80 g L^{-1} pH 3; (d) ovalbumin 20 g L^{-1} pH 10; (e) ovalbumin 40 g L^{-1} pH 10. (f) ovalbumin 80 g L^{-1} pH 10; (g) fibrinogen + thrombin 2 g L^{-1} pH 7.4; (h) fibrinogen + thrombin 4 g L^{-1} pH 7.4; (i) fibrinogen + thrombin 6 g L^{-1} pH 7.4.

ovalbumin hydrogel at pH 10 with an increase in protein concentration. The increase is more acute for the fibrinogen gel, a near 45% as the thrombin concentration increased from 2 to 6 g L^{-1}.

Understanding these phenomena requires a deeper knowledge of the microscopic processes involved in the interactions of individuals protein molecules between themselves and their environment. Gelation occurs because of the formation of inter- and intramolecular interactions among the protein chains, including hydrophobic interactions and hydrogen bonds.[37] When protein loses its native structure, this result in rapid aggregation and the formation of non-homogeneous microstructures resulting in gels with variable pore sizes.[38] Conformational changes of ovalbumin involved the formation of stable intermolecular beta-sheet structure. However, the ovalbumin did not take on a random-coiled structure but rather retained a considerable amount of secondary structure. The formation of intermolecular disulfide bonds may play a role in the formation of these gels. SANS studies have indicated that some of the denatured ovalbumins form a gel network and the others do large clusters with an interparticle distance of 250 Å. This complexity can induce an inhomogeneous organization in the gel structure.[23] The structural properties of ovalbumin are dependent on several external factors: pH, concentration of protein, dispersion, oil-phase volume and presence of salts. However, the pH was the most important one. The surface hydrophobicity of ovalbumin was greater at acidic pHs than at other pHs. No significant difference was found between the secondary structure of ovalbumin at pH 3 and that at pH 7, but microenvironmental changes were shown around the aromatic amino acid residues in acid solution. It was suggested that the globular conformation and secondary structure of ovalbumin may be almost the same at acidic and neutral pHs.[39] However, the side chains in the molecule are more flexible at lower pHs than at higher pHs, and they are very susceptible to denaturation.[40] At high pH, ovalbumin is highly charged and this affects not only the intermolecular interaction between ovalbumin molecules, but also the intramolecular interaction within the surrounding molecules. Consequently, electrostatic repulsion is weaker at pH 3 which results in a more compact structure of the gel. Increasing concentrations of protein becomes intermolecular disulfide bonds more relevant, resulting in a decrease in the mean pore area and wall thickness. The above observations are consistent with the results of earlier solution studies.[41]

Regarding the fibrin hydrogels, these are formed from soluble fibrinogen which are converted into insoluble fibrin through thrombin-mediated fibrinopeptide release. The activated fibrin molecules then self-assembled into a linear array, protofibril. The protofibrils also aggregate laterally in presence of factor XIII forming thicker fibers and eventually a stabilized 3D network of fibrils known as the fibrin clot.[42] The fibrin clot's primary microstructure consists of a disordered network of entangled, branching fibrin fibers. Thinner fibers are associated with networks which display an increased number of branch

points creating denser, less permeable clots. More open networks are formed from thicker fibers, the latter displaying a reduced number of branch points for a given amount of fibrinogen and producing a more porous system.[43] Also, the formation of covalent bonds is not necessary for gelation of fibrin but it does result in a more rigid elastic network.[44–47] As seen in Fig. 1g to i, with an increase in the concentration of thrombin there is an increase in the number of porous. This observation suggests that thrombin influences the rate of linear polymerization of fibrils to that of the lateral aggregation of protofibrils, where high thrombin concentration leads to thinner fibers and more porous gels.[43]

On the other hand, a fractal dimension can be quantified from SEM images of the hydrogels. To do this, the box counting method was applied to different SEM images.[32] This protocol consists of applying an increasingly fine grid over the area studied and counting at each iteration the number of boxes containing at least one part of the object to be measured. The fractal dimension D_f is then linked to the number $n(s)$ of boxes of dimension s necessary to fill the surface area of the particle according to:[48] $D_f = \lim_{s\to 0}(\ln n(s)/\ln(1/s))$. This method was also optimized by means of a calculation procedure stemming from the work of Foroutan-Pour *et al.*,[49] which allows a precise determination of the key parameters of the method, namely the number and the dimensions of the boxes.[50] The images, initially with 256 grey levels and 1024 × 768 pixels in size, are converted to binary images. The fractal dimension is then derived from the slope of a least-square linear fit of the plot of log *n versus* log (box size), where n is the number of non-overlapping equal boxes that would fill the projected surface area of the aggregate. Table 1 shows the values of the fractal dimensions obtained for all hydrogels under study. It is important to highlight that those values are obtained from the analysis of 2D images. Most authors, based on Minkowski–Bouligand dimension and the contents of projections on the directions of the planes, have demonstrated that, in general, there is no overall relationship between 3D and 2D fractal dimensions.[51] However, functional relationships between 2D and 3D fractal dimension were found for different systems,[52] assuming a uniform mass distribution of the object along the third dimension: $d_{3D} = 0.47d_{2D} + 1.78$.

Table 1 Fractal dimensions from the Box Counting method of the SEM images of all prepared hydrogels and their corresponding synthesized materials (estimated uncertainties ±0.002)

	Fractal dimensions	
System	Gels	Materials
OVO pH3 20 g L	1.807	1.746
OVO pH3 40 g L	1.811	1.764
OVO pH3 80 g L	1.839	1.817
OVO pH10 20 g L	1.814	1.703
OVO pH10 40 g L	1.878	1.728
OVO pH10 80 g L	1.895	1.815
FB Th2	1.787	1.808
FB Th6	1.794	1.820
FB Th8	1.824	1.834

D_f values listed in Table 1 lied well within the range of fractal dimension values reported for protein gels. Furthermore, comparison of these values with previously measured ones by other experimental techniques shows good agreement. Thus, Eleya *et al.* have found for ovalbumin gels low D_f values (1.9–2.1) for gels prepared at acidic and neutral pHs 3–7 whereas higher D_f values (2.2–2.4) were obtained for gels formed under basic pH conditions.[53] On the other hand, linear relationships between fractal dimensions and surfactant hydrophobicity have been found in ovalbumin plus surfactant gels,[54] suggesting similar mechanism of compactions. Regarding the fibrinogen-thrombin gels, our results also corroborate those previously found by means of viscoelastic measurements.[43] Hawkins and Evans have found that thrombin concentration influences the relative rate of linear polymerization of fibrin monomers to that of the lateral aggregation of protofibrils, this results in an increase of D_f with thrombin concentration.[55]

3.2. Mechanical characterization of the hydrogels

The ovalbumin and fibrin hydrogels were characterized mechanically in the linear viscoelastic region (LVR). The LVR is defined as the deformation range where the elastic modulus (G') is independent of deformation (γ%). After a critic deformation (γ%), elastic modulus exhibits a sharp change in its slope, decreasing as function of the deformation, which is indicative of the breakdown of the hydrogel microstructure. In order to measure the LVR for gel samples, oscillatory stress deformation sweeps were performed at a constant frequency (ω) of 10 rad s^{-1} and a temperature of 25 °C. Fig. 2 shows G' as a function of deformation and ovalbumin concentration for gels prepared at pH 3 (a) and pH 10 (b). Results indicate that for gels prepared at pH 3 (2a), the LVR shifts to lower deformations driving by the

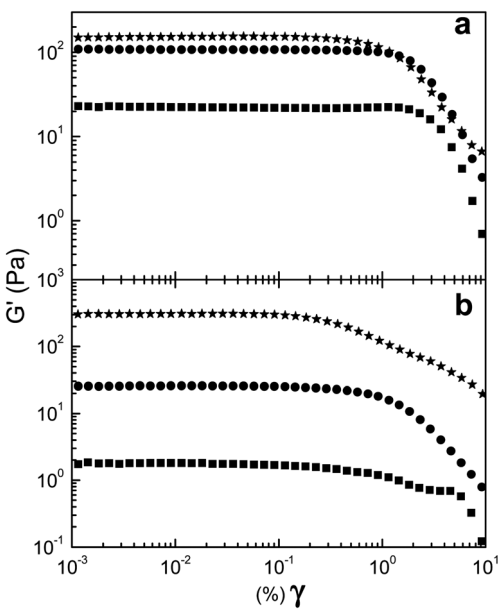

Fig. 2 Storage G' modulus obtained with strain sweep experiments performed at 10 rad s^{-1} and 25 °C for ovalbumin hydrogels synthesized at pH 3 (a) and pH 10 (b) for different ovalbumin concentration (g L^{-1}): (■), 10; (●), 20; (★), 30.

ovalbumin concentration. At the lowest ovalbumin concentration of 10 g L^{-1}, the LVR extends up to deformations values around 2%. While, for the higher concentration (30 g L^{-1}) the LVR diminishes up to around 0.1%. This indicates that inside the sample, there are micro domains constituting the hydrogel systems, *i.e.* existence of physical links between the micro domain and at the same time weak covalent bonds becoming more breakable when the concentration increases, even when the cross-linking density rises. This behavior could produce diminishing decrease in the resistance of hydrogel samples against deformation. Besides, tan δ ($=G''/G'$) value (not shown) of the gel samples increases indicating that samples become softer with ovalbumin concentration. For all hydrogels samples prepared at pH 10, the LVR extends up to deformations around 0.2%. This value is similar to that measured for the gel sample with 30 g L^{-1} obtained at pH 3, indicating similar breakable levels. Also, another difference of gel samples prepared at pH 10 is the relating G''/G' values, which did not exhibit any tendency with protein concentration.

Fig. 3, shows elastic modulus as a function of deformation and thrombin concentrations obtained in stress deformation sweeps at a frequency of 10 rad s^{-1} and a temperature of 25 °C. The linear viscoelastic region limit does not exhibit a tendency with thrombin concentration, the LVR extends up to about 1.8%. Nevertheless, in the strain-independent region, at a lower concentration, rigidity values were much lower than at the higher concentration, consequently, the gel strength is dependent on the thrombin concentration.

Fig. 4 shows the elastic and loss moduli as a function of frequency and OVO concentration obtained in frequency sweep experiments for samples prepared at pH 3 (a) and pH 10 (b). The applied deformation for both pH's hydrogels was 0.01% that is within the linear viscoelastic region and at a temperature of 25 °C. The elastic modulus for hydrogels prepared at pH 3 slightly rises with increasing frequency, but it is overall relatively constant. Such rheological behavior indicates the presence of permanent junction points as opposed to transient entanglements leading to a viscoelastic plateau.[56,57] It is evident in this figure that, the elastic and the loss moduli values

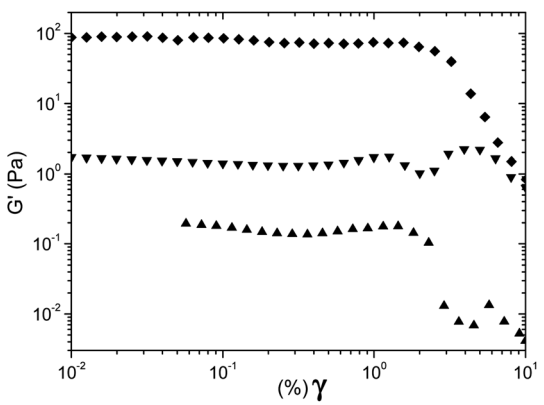

Fig. 3 Storage G' modulus obtained in strain sweeps experiments performed at 10 rad s^{-1} and 25 °C for fibrinogen + thrombin hydrogels synthesized at pH 7.3 for different thrombin concentrations (g L^{-1}): (▲), 2; (▼), 4; (◆), 6.

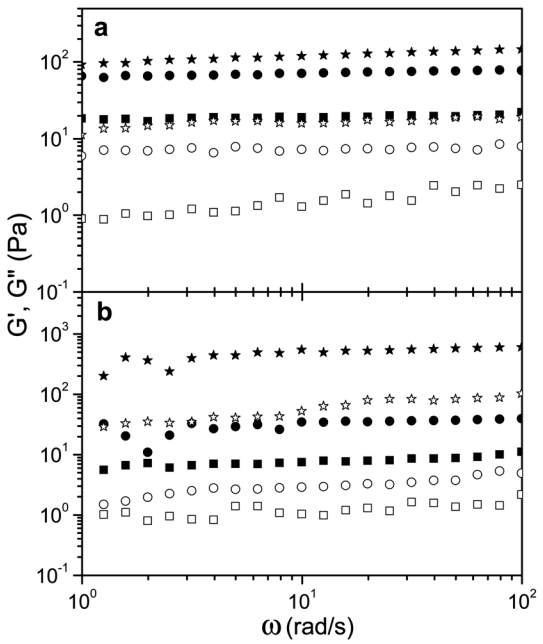

Fig. 4 Elastic G' (closed symbols) and loss G'' (open symbols) moduli obtained with frequency sweeps experiments performed at a deformation of 0.01% and 25 °C for ovalbumin hydrogels synthesized at pH 3 (a) and pH (10) for different ovalbumin concentration (g L^{-1}): (■), 10; (●), 20; (★), 30.

increase as the concentration increases. This could be due to the increase of the cross-linking density with increasing OVO concentrations. Besides, the elastic modulus is consistently larger than the loss modulus (G'') indicating that the hydrogels behave as a gel-like over the frequency range studied. Nevertheless, the relative increase in G' over G'' diminished as protein concentration augments, producing an increase in tan δ (dissipation capacity) as we show later. This causes that gels become softer and consequently decreases the mechanical properties. On the other hand, for gel samples prepared at pH 10 (Fig. 4b) the rheological behavior is similar to that observed for samples obtained at pH 3. However, the relative increase in G' over G'' did not have any tendency with protein concentration.

The dependence of both the elastic and viscous moduli of thrombin gels were determined as a function of concentration at 25 °C, with a deformation of 0.1% that is within the linear viscoelastic region are shown in Fig. 5. It is evident in this figure that over a broad range of frequencies the elastic modulus is essentially frequency independent for all samples. Elastic modulus increases as concentration of thrombin increases in similar way than that observed in hydrogel samples of OVO protein for both pH's, this may be due the increasing of the crosslinking density. However, a difference was observed, the relative increase in G' over G'' did not changes with thrombin concentration and the dissipation capacity values (tan δ) are lower than for all samples. This indicates that thrombin hydrogels samples are softer than those obtained with OVO protein.

The dependence in the log–log plot of elastic modulus as a function of OVO protein is shown in Fig. 6a for hydrogels

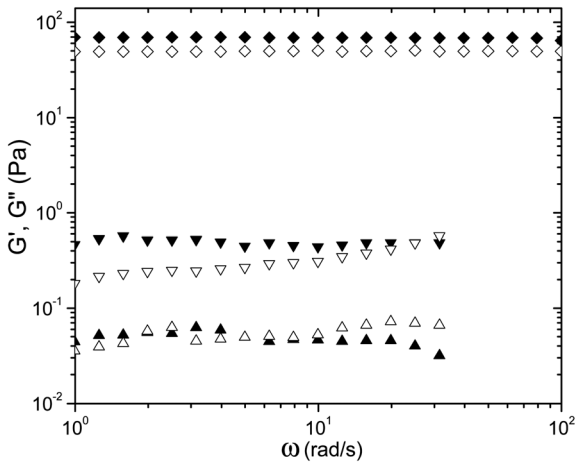

Fig. 5 Elastic G' (closed symbols) and loss G'' (open symbols) moduli measured in frequency sweeps experiments performed at a deformation of 0.01% and 25 °C for fibrinogen + thrombin hydrogels synthesized at pH 7.3 for different thrombin concentrations (g L^{-1}): (▲), 2; (▼), 4; (◆), 6.

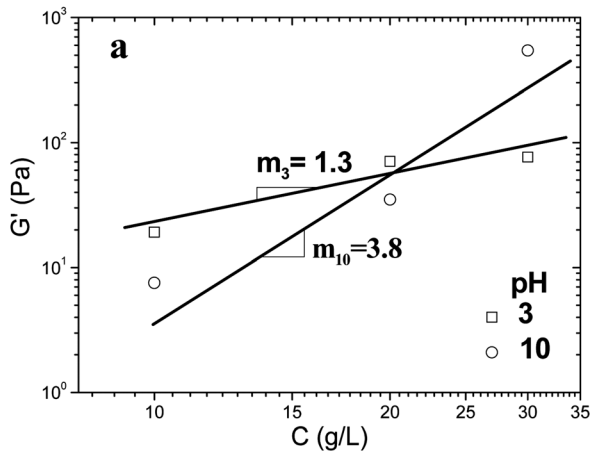

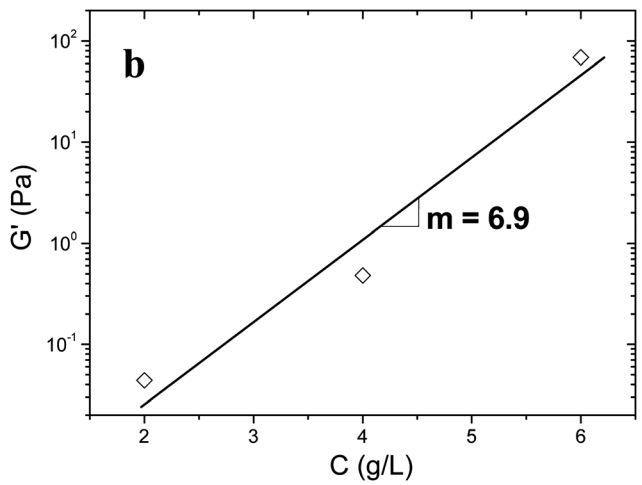

Fig. 6 Elastic modulus G′ at a frequency of 10 rad s^{-1} as a function of ovalbumin concentration (a) for hydrogel samples synthesized at pH 3 (□) and 10 (○), and (b) thrombin concentration (b) synthesized at pH 7.3.

obtained at pH 3 (open square) and 10 (open circles). Data was obtained at a frequency of 10 rad s^{-1}, in the linear viscoelastic region at 25 °C. Results indicates that for samples obtained at pH 10 G' exhibits a larger dependence with protein concentration ($m \sim 3.8$) than those obtained at pH 3 ($m \sim 1.3$). A relationship between G' and concentration of protein and polysaccharides gels corresponding C^2 was reported for Clark and Ross-Murphy.[58] MacKintosh *et al.*[56] proposed a model for densely cross-linked actin proteins. They showed that the elastic modulus scaled with concentration as

$$G' \propto C^A \quad (1)$$

with $A = 2.2$. Similar power law exponents were reported for hydrogels based on coarse fibrin networks,[46] F-actin[56] and for oligopeptides.[57] Recently Hassan *et al.*,[32] reported a power law exponent value of 3.5 for hydrogel of bovine plasma fibrinogen. The slope of 1.3 for hydrogel prepared at pH 3 is lower than that predicted by eqn (1). For hydrogel samples prepared at pH 10, the slope 3.8 is higher than that reported for fibrinogel hydrogel but lower than that reported for hydrogels based on oligomers electrolytes (4.5).[59] It is evident in this figure that for concentrations ≤ than 20 g L^{-1}, hydrogel samples prepared at pH 3 showed larger G' values than those prepared at pH 10. This suggests that samples prepared at pH 3 in this concentration interval are more highly cross-linked than those prepared at pH 3. At higher concentrations, hydrogel samples prepared at pH 10 with protein concentration of 30 g L^{-1}, exhibited a higher G' value than that obtained at pH 3, indicating that the sample became more cross-linked. On the other hand, hydrogel samples based on thrombin, exhibited a slope $m \sim 6.9$, that is larger than all the power law dependence reported.

In Fig. 7, the dependence of tan δ values (dissipation capacity) as a function of protein OVO concentration for hydrogel samples prepared at pH 3 at a frequency of 10 rad s^{-1}. It is evident in this figure that tan δ increases with protein concentration, indicating that samples become softer as

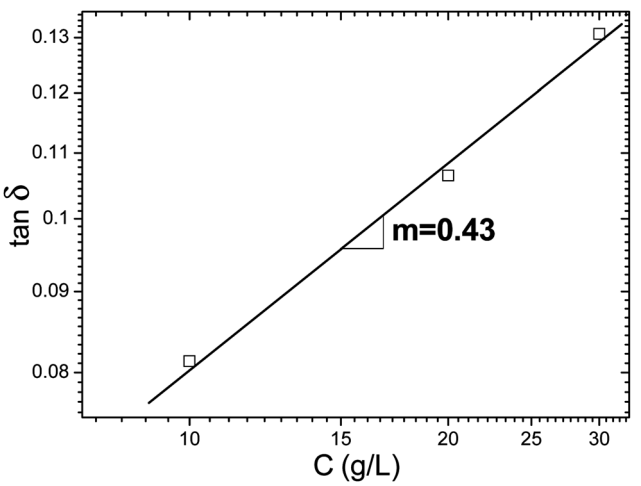

Fig. 7 Tan δ at a frequency of 10 rad s^{-1} as a function of ovalbumin concentration for hydrogels synthesized at pH 3 and 25 °C.

concentration increases. This rheological behavior is opposing to that observed in hydrogels synthesized with fibrinogen.[32]

3.3. Biotemplating of silica architectures

The architecture of the silica structures synthesized from the gels was also examined using SEM. Fig. 8 shows SEM micrographs of the final structures obtained from the corresponding gels. The two first rows show the morphology of the different silica mesophase structures formed with increasing ovalbumin concentration at pH 3 (Images 8a to 8c) and pH 10 (Images 8d to 8f) respectively. Both series exhibit similar features: hierarchical roughness and high porosity. No real spheres are observed, the same irregular morphology is found for both pH. When the concentration of protein is further increased, a change occurs: the silica structure is more open. Silica precursor is believed to be entrapped in the hydrogel nanopores which functions as a diffusion barrier. Images 8a to 8c display that the surface is relatively smooth and has few sites that can trap silica. However, the perceptible disparity in the surface morphology of ovalbumin gels at pH 3 and pH 10 contrasts with the similarity of the silica structures obtained from both pHs. This fact can be explained taking into account that ovalbumin has a higher content of cysteine. This amino acid has little ability to attract and align nuclei, but rather acts only as a catalyst for the hydrolysis of silica precursors.[60] The isoelectric point of cysteine is 5.07. Therefore, the advantage of the gels with more open structures (pH 10) is compensated by a higher catalytic activity of cysteine at pH below the isolectric point (pH 3), resulting in similar silica structures at both pHs.

Scanning electron microscopy images of samples created from fibrinogen-thrombin gels (Fig. 8g to i) show that the material is composed of small regular particles of spherical shape with average sizes of about 2 nm that are aggregated into clusters. There were no higher ordered structures or differences of statistical significance in average size of particles with increase in thrombin concentration. As all particles are spherical presumably they are formed by homogeneous nucleation. The only possible effect that changes with thrombin increasing concentrations is that the particles tend to aggregate loosely.

It was recently reported the preparation of silica nanostructures through a hydrogel matrix formed from just fibrinogen, the final materials show two different topologies: sponge-like and polygonal fibers. The origin of these two topologies lies on the anisotropic shape of the fibrinogen, driving stochastic interactions with the silica precursor.[32] However, in this study the presence of thrombin in the gel results in a silica structure with a single and homogeneous morphology.

The amorphous character of all these structures were simultaneously corroborated from high-resolution powder X-ray diffraction experiments that showed no discernible peaks and high-resolution TEM micrograph (data not shown), confirming that the samples are indeed fully amorphous. Among other biogenic minerals, silica appears rather singular.

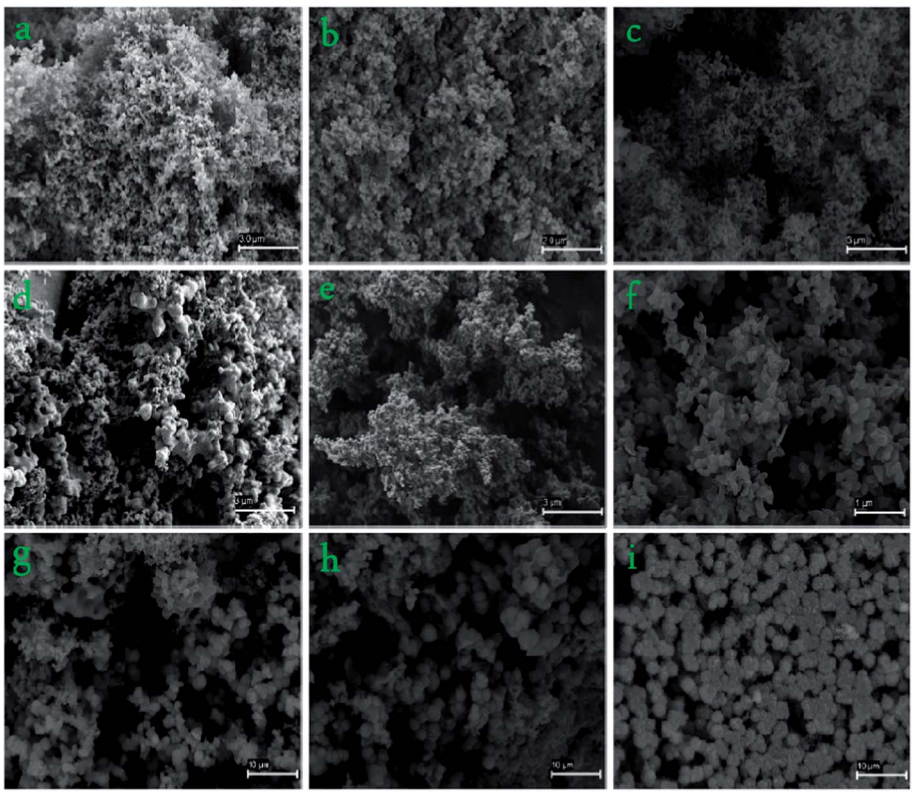

Fig. 8 SEM micrographs of the various morphologies present in templated silica structures prepared from hydrogels produced at different conditions: (a) ovalbumin 20 g L^{-1} pH 3; (b) ovalbumin 40 g L^{-1} pH 3; (c) ovalbumin 80 g L^{-1} pH 3; (d) ovalbumin 20 g L^{-1} pH 10; (e) ovalbumin 40 g L^{-1} pH 10. (f) ovalbumin 80 g L^{-1} pH 10; (g) fibrinogen + thrombin 2 g L^{-1} pH 7.4; (h) fibrinogen + thrombin 4 g L^{-1} pH 7.4; (i) fibrinogen + thrombin 6 g L^{-1} pH 7.4.

Carbonate and phosphate salts are crystalline ionic or covalent solids whose precipitation is dictated by solubility equilibrium. In contrast, silica is an amorphous metal oxide formed by a more complex inorganic polymerization processes.[61] Furthermore, the amorphous nature of the synthesized materials can also be related to strong dipolar interactions.[62,63]

Focusing now on the fractal analysis, SEM images presented in Fig. 8 suggested that silica structures exhibited a branched and self-similar appearance formed by fractal agglomerates, which were constituted of primary individual silica particles. Accordingly, we have calculated the fractal dimension of the silica structures following the imaging procedure that was already discussed. The obtained values can be observed in Table 1. These values indicate that fractal dimension of silica structures follow the same pattern that their corresponding templates as concentration increases. Importantly, whereas the dimensions of the materials obtained from ovalbumin gels are always smaller than their corresponding templates, we observed an opposed pattern in the case of fibrinogen. The fractal dimensions of silica structures obtained by different routes have been recently calculated. Thus, Wu *et al.* by using an ionic liquid as a solvent at different ratios and SAXS measurements have obtained values between 1.3 and 1.8. The smallest value corresponds to a highly porous network, while the largest to a collapsed one.[64] Mohite *et al.*[65] by means of polymer-cross-linked systems reach a value of 1.9, at this point, silica structures are quite robust materials. All our values are between 1.70 and 1.83, corresponding to a relatively porous material easy to handle.

4. Conclusions

In this work, we have designed a route to synthesize protein hydrogel of ovalbumin and fibrinogen for the subsequent synthesis of biotemplating of silica architectures, The morphology of the protein hydrogels depend on the environment pH, when the pH of the protein is close to the pI, the arquitecture of the hydrogel is a monolithic and compact structure for ovalbumin and fibrinogen, respectively. Nevertheless, in hydrogels synthesized at pHs far from the pI the arquitectures results in more open structures. The size of the pores of the hydrogels decrease when the protein concentration increases, from to 15.8 to 8.5 μm^2 and 63.6 to 17.1 μm^2 in the case of ovalbumin and thrombin respectively. Also, when the protein concentration changes, the hydrogel wall thickness decreases with the concentration. The dissipation capacity values decrease with protein concentration indicating that samples becoming softer, nevertheless this rheological behavior is not the same for hydrogels synthesized with fibrinogen. The obtained silica architectures from protein hydrogels are protein and pH dependent. However, exhibit some common features, hierarchical roughness and high porosity. The fractal dimension of the silica structures followed the same pattern that the templates, when the concentration is increased the fractal dimension increases. Accordingly with these results, the method proposed here provides a new route to synthesize silica nanostructures with defined three dimensional dimensions, representing a very simple and fast strategy under green conditions.

Acknowledgements

The authors acknowledge: Xunta de Galicia (Project no. 10PXIB206258PR), MICINN-Spain (MAT2011-25501) and Universidad Nacional del Sur (PGI 24/ZQ07), Concejo Nacional de Investigaciones Científicas y Técnicas de la República Argentina (CONICET, PIP-11220100100072).

References

1 F. C. Meldrum and H. Cölfen, *Chem. Rev.*, 2008, **108**, 4332–4432.
2 M. B. Dickerson, K. H. Sandhage and R. R. Naik, *Chem. Rev.*, 2008, **108**, 4935–4978.
3 M. S. Bakshi, H. Kaur, P. Khullar, T. S. Banipal, G. Kaur and N. Singh, *J. Phys. Chem. C*, 2011, **115**, 2982–2992.
4 A. E. Stephenson, J. J. DeYoreo, L. Wu, K. J. Wu, J. Hoyer and P. M. Dove, *Science*, 2008, **322**, 724–727.
5 J. Seto, Y. Ma, S. A. Davis, F. Meldrum, A. Gourrier, Y.-Y. Kim, U. Schilde, M. Sztucki, M. Burghammer, S. Maltsev, C. Jäger and H. Cölfen, *Proc. Natl. Acad. Sci. U. S. A.*, 2012, **109**, 3699–3704.
6 Y. Wang, T. Azaïs, M. Robin, A. Vallée, C. Catania, P. Legriel, G. Pehau-Arnaudet, F. Babonneau, M.-M. Giraud-Guille and N. Nassif, *Nat. Mater.*, 2012, **11**, 724–733.
7 L. Wang and M. Nilsen-Hamilton, *Front. Biol.*, 2012, 1–13.
8 A. P. Schoen, D. T. Schoen, K. N. L. Huggins, M. A. Arunagirinathan and S. C. Heilshorn, *J. Am. Chem. Soc.*, 2011, **133**, 18202–18207.
9 C. Aime, G. Mosser, G. Pembouong, L. Bouteiller and T. Coradin, *Nanoscale*, 2012, **4**, 7127–7134.
10 S. Heinemann, T. Coradin and M. F. Desimone, *Biomater. Sci.*, 2013, **1**, 688–702.
11 W. R. Algar, D. E. Prasuhn, M. H. Stewart, T. L. Jennings, J. B. Blanco-Canosa, P. E. Dawson and I. L. Medintz, *Bioconjugate Chem.*, 2011, **22**, 825–858.
12 G. Acharya, M. McDermott, S. J. Shin, H. Park and K. Park, *Methods Mol. Biol.*, 2011, **726**, 179–185.
13 W. Mulyasasmita, J. S. Lee and S. C. Heilshorn, *Biomacromolecules*, 2011, **12**, 3406–3411.
14 C. Y. Khripin, D. Pristinski, D. R. Dunphy, C. J. Brinker and B. Kaehr, *ACS Nano*, 2011, **5**, 1401–1409.
15 E. Gianotti, U. Diaz, S. Coluccia and A. Corma, *Phys. Chem. Chem. Phys.*, 2011, **13**, 11702–11709.
16 A. C. Fournier and K. M. McGrath, *Soft Matter*, 2011, **7**, 4918–4927.
17 Y. Shchipunov and N. Shipunova, *Colloids Surf., B*, 2008, **63**, 7–11.
18 K. Broersen, A. M. M. Van Teeffelen, A. Vries, A. G. J. Voragen, R. J. Hamer and H. H. J. De Jongh, *J. Agric. Food Chem.*, 2006, **54**, 5166–5174.
19 Y. Sun and S. Hayakawa, *J. Agric. Food Chem.*, 2002, **50**, 1636–1642.

20 E. Tatsumi, D. Yoshimatsu and M. Hirose, *Biochemistry*, 1998, **37**, 12351–12359.
21 R. A. Judge, M. R. Johns and E. T. White, *J. Chem. Eng. Data*, 1996, **41**, 422–424.
22 B. Egelandsdal, *J. Food Sci.*, 1980, **45**, 570–574.
23 M. Sugiyama, A. Nakamura, N. Hiramatsu, M. Annaka, S. Kuwajima and K. Hara, *Biomacromolecules*, 2001, **2**, 1071–1073.
24 N. Murthy, M. Xu, S. Schuck, J. Kunisawa, N. Shastri and J. M. J. Fréchet, *Proc. Natl. Acad. Sci. U. S. A.*, 2003, **100**, 4995–5000.
25 S. Yakovlev and L. Medved, *Biochemistry*, 2009, **48**, 5171–5179.
26 J. H. Brown, N. Volkmann, G. Jun, A. H. Henschen-Edman and C. Cohen, *Proc. Natl. Acad. Sci. U. S. A.*, 2000, **97**, 85–90.
27 G. Tsurupa, R. R. Hantgan, R. A. Burton, I. Pechik, N. Tjandra and L. Medved, *Biochemistry*, 2009, **48**, 12191–12201.
28 N. Hassan, L. R. S. Barbosa, R. Itri and J. M. Ruso, *J. Colloid Interface Sci.*, 2011, **362**, 118–126.
29 N. Hassan, J. Maldonado-Valderrama, A. P. Gunning, V. J. Morris and J. M. Ruso, *Colloids Surf., B*, 2011, **87**, 489–497.
30 N. Hassan, J. Madonado-Vaderrama, A. P. Gunning, V. J. Morris and J. M. Ruso, *J. Phys. Chem. B*, 2011, **115**, 6304–6311.
31 N. Hassan, J. M. Ruso and P. Somasundaran, *Colloids Surf., B*, 2011, **82**, 581–587.
32 N. Hassan, A. Soltero, D. Pozzo, P. V. Messina and J. M. Ruso, *Soft Matter*, 2012, **8**, 9553–9562.
33 S. Ikeda, E. A. Foegeding and T. Hagiwara, *Langmuir*, 1999, **15**, 8584–8589.
34 P. Messina, M. Morini and P. Schulz, *Colloid Polym. Sci.*, 2004, **282**, 1063–1066.
35 G. R. Souza, E. Yonel-Gumruk, D. Fan, J. Easley, R. Rangel, L. Guzman-Rojas, J. H. Miller, W. Arap and R. Pasqualini, *PLoS One*, 2008, **3**, e2242.
36 C. Pecharromán, F. Esteban-Betegón, J. F. Bartolomé, G. Richter and J. S. Moya, *Nano Lett.*, 2004, **4**, 747–751.
37 U.-J. Kim, J. Park, C. Li, H.-J. Jin, R. Valluzzi and D. L. Kaplan, *Biomacromolecules*, 2004, **5**, 786–792.
38 W. Ho, B. Tawil, J. C. Y. Dunn and B. M. Wu, *Tissue Eng.*, 2006, **12**, 1587–1595.
39 T. Koseki, N. Kitabatake and E. Doi, *J. Biochem.*, 1988, **103**, 425–430.
40 Y. Mine, T. Noutomi and N. Haga, *J. Agric. Food Chem.*, 1991, **39**, 443–446.
41 N. Yuno-Ohta, T. Higasa, E. Tatsumi, H. Sakurai, R. Asano and M. Hirose, *J. Agric. Food Chem.*, 1998, **46**, 4518–4523.
42 A. des Rieux, A. Shikanov and L. D. Shea, *J. Controlled Release*, 2009, **136**, 148–154.
43 K. Hawkins, P. A. Evans, M. Lawrence, D. Curtis, M. Davies and P. R. Williams, *Rheol. Acta*, 2010, **49**, 891–900.
44 I. K. Piechocka, R. G. Bacabac, M. Potters, F. C. MacKintosh and G. H. Koenderink, *Biophys. J.*, 2010, **98**, 2281–2289.
45 A. E. X. Brown, R. I. Litvinov, D. E. Discher, P. K. Purohit and J. W. Weisel, *Science*, 2009, **325**, 741–744.
46 K. M. Weigandt, D. C. Pozzo and L. Porcar, *Soft Matter*, 2009, **5**, 4321–4330.
47 K. M. Weigandt, L. Porcar and D. C. Pozzo, *Soft Matter*, 2011, **7**, 9992–10000.
48 A. Giorgilli, D. Casati, L. Sironi and L. Galgani, *Phys. Lett. A*, 1986, **115**, 202–206.
49 K. Foroutan-pour, P. Dutilleul and D. L. Smith, *Appl. Math. Comput.*, 1999, **105**, 195–210.
50 S. Bau, O. Witschger, F. Gensdarmes, O. Rastoix and D. Thomas, *Powder Technol.*, 2010, **200**, 190–201.
51 H. Akkari, I. Bhouri, P. Dubois and M. H. Bedoui, *Math. Modell. Nat. Phenom.*, 2008, **3**, 48–75.
52 S. Ganguly, S. Basu and S. Sikdar, *Proc. Inst. Mech. Eng., Part N*, 2012, **226**, 3–7.
53 M. M. Ould Eleya, S. Ko and S. Gunasekaran, *Food Hydrocolloids*, 2004, **18**, 315–323.
54 N. Hassan, P. V. Messina, V. I. Dodero and J. M. Ruso, *Int. J. Biol. Macromol.*, 2011, **48**, 495–500.
55 P. A. Evans, K. Hawkins, R. H. K. Morris, N. Thirumalai, R. Munro, L. Wakeman, M. J. Lawrence and P. R. Williams, *Blood*, 2010, **116**, 3341–3346.
56 F. C. MacKintosh, J. Käs and P. A. Janmey, *Phys. Rev. Lett.*, 1995, **75**, 4425–4428.
57 B. Ozbas, K. Rajagopal, J. P. Schneider and D. J. Pochan, *Phys. Rev. Lett.*, 2004, **93**, 268106.
58 A. Clark and S. Ross-Murphy, in *Biopolymers*, Springer, Berlin Heidelberg, 1987, vol. 83, ch. 2, pp. 57–192.
59 S. K. Kundu, M. Yoshida and M. Shibayama, *J. Phys. Chem. B*, 2010, **114**, 1541–1547.
60 K. M. Roth, Y. Zhou, W. Yang and D. E. Morse, *J. Am. Chem. Soc.*, 2004, **127**, 325–330.
61 D. M. Nelson, P. Tréguer, M. A. Brzezinski, A. Leynaert and B. Quéguiner, *Global Biogeochem. Cycles*, 1995, **9**, 359–372.
62 V. C. Yee, K. P. Pratt, H. C. F. Côté, I. L. Trong, D. W. Chung, E. W. Davie, R. E. Stenkamp and D. C. Teller, *Structure*, 1997, **5**, 125–138.
63 M. Brinkmann, G. Gadret, M. Muccini, C. Taliani, N. Masciocchi and A. Sironi, *J. Am. Chem. Soc.*, 2000, **122**, 5147–5157.
64 C.-M. Wu, S.-Y. Lin and H.-L. Chen, *Microporous Mesoporous Mater.*, 2012, **156**, 189–195.
65 D. P. Mohite, Z. J. Larimore, H. Lu, J. T. Mang, C. Sotiriou-Leventis and N. Leventis, *Chem. Mater.*, 2012, **24**, 3434–3448.